Open Access Journal
Journal of Power Technologies 93 (5) (2013) 288–294
journal homepage:papers.itc.pw.edu.pl

Research on steam condensing flows in nozzles with shock wave

Sławomir Dykas*, Mirosław Majkut, Krystian Smołka, Michał Strozik

Institute of Power Engineering and Turbomachinery
Silesian University of Technology, Gliwice, Poland

Abstract

The paper presents experimental and numerical results of steam transonic flows in Laval nozzles. The geometries of half arc nozzles were used in testing. Subject to investigation was the behavior of shock waves in the wet steam region. Due to high back pressure the shock wave was created in the divergent part of the nozzle, and interaction with the nozzle walls caused instability in the flow. The experimental results were compared with numerical calculations of steam condensing transonic flow.

Keywords: wet steam, experiment, CFD, transonic flows

1. Introduction

In large output turbines, the state path usually crosses the saturation line in the penultimate stages [1]. This means that at least last two stages of the low-pressure turbine operate in the two-phase region, producing much more than 10% of the total power output. The liquid phase in steam turbines is mainly created in the process of homogeneous and heterogeneous condensation. The part of the heterogeneous condensation in liquid phase formation depends on steam purity. For the purposes of the problems considered in this paper it was assumed that the steam was perfectly pure.

The flow in the low-pressure steam turbine is complicated and still requires thorough experimental and numerical analysis to increase energy conversion efficiency. Low-pressure turbine blades are key components in overall steam turbine design. A fully developed 3-D stage flow analysis can provide an optimum blade profile, capable of minimizing losses from shock waves caused by supersonic flow and also from condensation shocks. The accuracy of modern 3-D analysis as a prediction tool has improved considerably and it can now account for non-equilibrium condensation flows with different steam wetness conditions and phase change variations.

However, more experimental research on steam condensing flow is required, especially for simple geometry like Laval nozzles. The most of the experimental data used for validation of the numerical models is relatively old [2–4] and does not include a precise investigation of shock wave behavior in the wet steam regime. Usually, validation of the numerical models against experimental data for nozzles did not consider this problem [5–7].

The aim of this paper is to prove that the shock wave in the wet steam flow may be responsible for instabilities that are not observed in aerodynamic experiments and calculations. The reason for that is the presence of the thin liquid films on the solid walls that are separated due to their interaction with the shock wave.

The presented experimental and numerical research

*Corresponding author
Email address: slawomir.dykas@polsl.pl (Sławomir Dykas*)

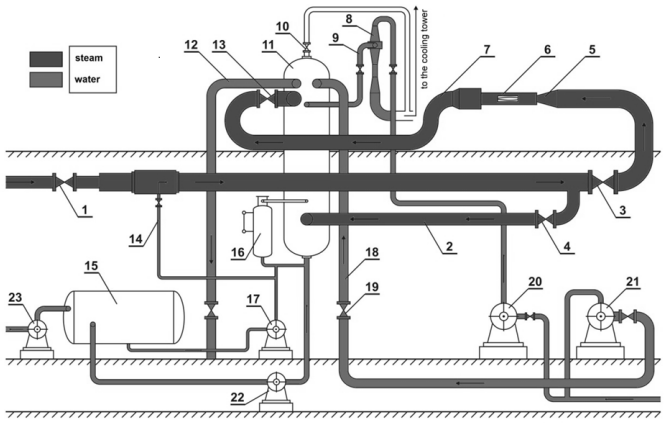

Figure 1: Steam tunnel with auxiliary devices: 1) Control valve, 2) By-pass, 3) Stop gate valve, 4) Stop gate valve at by-pass, 5) Inlet nozzle, 6) Test section, 7) Outlet elbow, 8) Water injector, 9) Pipe, 10) Safety valve, 11) Condenser, 12) Suction line, 13) Throttle valve, 14) Desuperheater, 15) Condensate tank, 16) Control system of condensate level, 17) Condensate pump, 18) Discharge line, 19) Stop valve, 20) Water injector pump, 21) Cooling water pump, 22) Condensate pump, 23) Pump

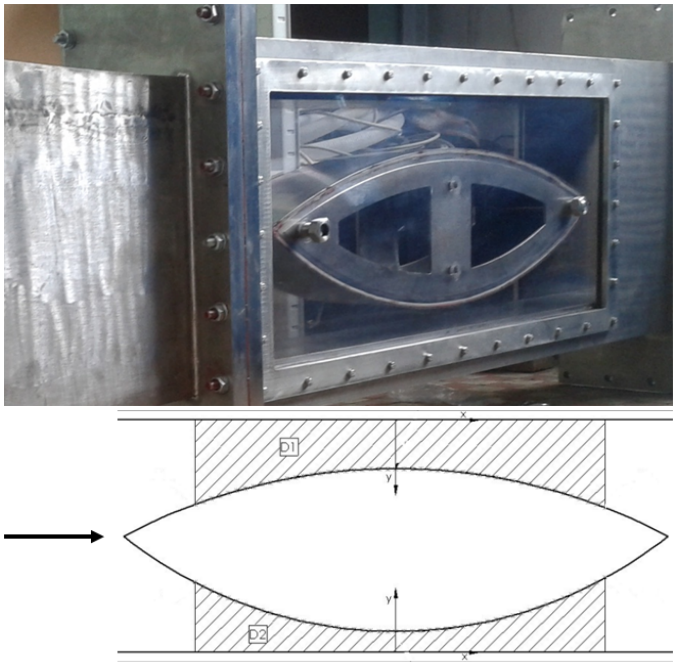

Figure 2: The photo (top) and the geometry (bottom) of the test section with two half nozzles

was carried out using the in-house facility and in-house numerical CFD code.

2. Experimental facility

The experimental facility is part of the small steam condensing power station located in the Institute of Power Engineering and Turbomachinery of the Silesian University of Technology. The steam tunnel facility (Fig. 1) was designed to perform experiments for steam condensing flows in nozzles or linear cascades [8]. Superheated steam with very stable parameters is supplied from the 1 MW_t boiler. The maximum steam mass flow rate is about 3 kg/s. The parameters ahead of the test section are controlled by means of a control valve and desuperheater, providing the steam with parameters corresponding to the conditions prevailing in low-pressure turbine stages. The total inlet pressure range is 70...150 kPa(a) and total temperature range is 70...120 °C.
In the test section two half arc Laval nozzles were installed (Fig. 2). The D1 half nozzle is an arc nozzle with critical throat height of 55.5 mm and wall curvature radius of 700 mm. The second half nozzle, the D2 nozzle, is also an arc nozzle with lower critical throat height of 27.5 mm and wall curvature radius of 525 mm. The width of the nozzles was 110 mm.

The static pressure measurement in the nozzles was carried out at a distance of 200 mm downstream from the critical throat, along the center line of the nozzle width. The distance between pressure taps was 10 mm. Each measurement series lasted 30 seconds and static pressure was measured with the frequency of 400 Hz, which gave 12,000 samples. The accuracy of the applied pressure transducers was ±100 Pa.
Measurement accuracy within one series was calculated as the difference between the maximum and minimum values plus the accuracy of the sensor.

3. Numerical model

The numerical calculations were performed using TranCoFlow in-house CFD code based on URANS equations coupled with two equations $k-\omega$ SST viscous turbulence for the vapor/liquid mixture [9, 10].
It is assumed in the numerical model that the two phases are governed by the same pressure:

$$p = p_v = p_l \tag{1}$$

The following relationships connect the liquid and the vapor phase:

$$\begin{aligned} \alpha &= \tfrac{V_l}{V_m} \\ \rho_m &= (1-\alpha)\,\rho_v + \alpha\rho_l \\ h_m &= (1-y)\,h_v + y h_l \\ y &= \alpha\tfrac{\rho_l}{\rho_m} \end{aligned} \qquad (2)$$

where α is the volume fraction and y is the mass fraction of the liquid phase. Mixture density ρ_m is a function of vapor density ρ_v, liquid density ρ_l, and α. Mixture enthalpy h_m is determined in a similar way. Mass fraction y depends on the volume fraction as well as on the ratio between the liquid and the mixture density. For the presented problem its value is approx. 10^3 higher than that of the volume fraction.

The applied state equation for the gas phase takes a very complex form and is practically useless for direct application to CFD codes. In the presented in-house CFD code the 'local' real gas state equation is used in a form similar to the virial equation of state with one virial coefficient [5]:

$$\frac{p}{RT_v\rho_v} = z\,(T_v,\rho_v) = A(T_v) + B(T_v)\rho_v, \qquad (3)$$

where p, v, T are pressure, specific volume and temperature, respectively, $R = 416.5\ J/(kg\ K)$ is the gas constant, z stands for the compressibility coefficient and polynomials $A(T)$, $B(T)$ are of the second order.

The nucleation model presented in this study is the homogenous one. In this kind of nucleation, condensation occurs without the influence of impurities or surfaces. In the supersonic region, if the flow is heated by latent heat of the condensation process, its velocity decreases and its pressure increases. As a result, a condensation shock (or rise in pressure) occurs, which increases the flow entropy producing local losses.

In the presented models, the homogeneous condensation phenomenon is modeled on the basis of classical nucleation [11] and the continuous droplet growth model [4].

The nucleation rate, i.e., the number of supercritical droplets produced per mass unit of vapor per time unit, is calculated from the relation obtained through the classical nucleation theory. This relation is derived from the assumption of a thermodynamic equilibrium between critical droplets and vapor:

$$J_{hom} = C\sqrt{\frac{2\sigma}{\pi}}m^{-3/2}\frac{\rho_v}{\rho_l}\exp\left(-\beta\frac{4\pi r^{*2}\sigma}{3kT_v}\right) \qquad (4)$$

where coefficient C is the non-isothermal correction factor proposed by Kantrowitz [12] (the isothermal model assumption does not apply to vapor), which is calculated from the relation:

$$C = \left[1 + 2\frac{\gamma-1}{\gamma+1}\frac{h_v-h_l}{RT_v}\left(\frac{h_v-h_l}{RT_v} - \frac{1}{2}\right)\right]^{-1} \qquad (5)$$

and s is the surface tension, m the mass of a single water molecule and β the correction factor (in the presented calculations $\beta = 1$).

The radius of critical clusters $r*$ was calculated taking into account the vapor state equation (Eq. 3). Further behavior of critical droplets can be described by appropriate droplet growth law. Once the droplets are formed, they increase in size as vapor molecules condense on their surfaces. The energy released in condensation leads to a rise in the temperature of the droplets, and hence the droplets become hotter than the surrounding vapor during the condensation process. Droplet growth is thus governed mainly by the mass transfer towards the droplet and the energy flux away from it. In pure vapor, however, due to the release of very high latent heat in the rapid condensation zone, droplet growth is dominated by the thermal transfer rate.

The Knudsen number Kn plays a key role in the coefficient of the heat transfer due to the wide range of the radii of the droplets. The Knudsen number is the ratio of the mean free path of vapor molecules to droplet diameter $Kn \equiv \bar{l}/2r$.

The size of droplets for vapor under low pressure is much smaller than the mean free path of vapor molecules. Therefore, droplet growth should be governed by considering the molecular and macroscopic transport process (Hertz-Knudsen model). Problems with the choice of condensation and accommodation coefficients make application of the Hertz-Knudsen model very difficult for calculations. This difficulty can be avoided by using the Gyarmathy droplet growth model, which takes into account the diffusion of vapor molecules through the surrounding vapor as well as the heat and mass transfer, and the influence of capillarity:

$$\frac{dr_{hom}}{dt} = \frac{1}{\rho_l}\frac{\lambda_v}{(1+3.18Kn)}\frac{r-r^*}{r^2}\frac{T_s-T_v}{h_v-h_l}. \qquad (6)$$

In the presented models the phase change is represented by two mass sources, according to the relations:

$$\begin{aligned}\Gamma_1 &= \tfrac{4}{3}\pi\rho_l\rho_m r_{hom}^{*3} J \\ \Gamma_2 &= 4\pi\rho_l\rho_m n_{hom} r_{hom}^2 \tfrac{dr_{hom}}{dt}\end{aligned}, \quad (7)$$

where Γ_1 is the mass source of critical droplets of the mass created due to the nucleation process, and Γ_2 is the mass condensation rate of all droplets per volume unit of the two-phase mixture (kg/m^3s) for homogeneous condensation, where n is the concentration of liquid droplets per unit mass.

A typical approach used for the analysis of two-phase flows is the single fluid (mixture) model, i.e. the individual fluid phases are assumed to behave as a flowing mixture described in terms of the mixture's properties. The applied single-fluid model consists of two equations describing the formation and growth of the liquid phase resulting from homogeneous condensation:

$$\begin{aligned}\tfrac{\partial(\rho_m y_{\mathrm{hom}})}{\partial t} + \tfrac{\partial(\rho_m u_{mj} y_{hom})}{\partial x_j} &= \Gamma_1 + \Gamma_2 \\ \tfrac{\partial(\rho_m n_{hom})}{\partial t} + \tfrac{\partial(\rho_m u_{mj} n_{hom})}{\partial x_j} &= \rho_m J\end{aligned} \quad (8)$$

where:

$$E_m = h_m - \frac{p}{\rho_m} + \frac{1}{2}u_{mj}u_{mj} \quad (9)$$

is the specific total internal energy of the mixture.

Pressure p has to be calculated from the relation for the total energy of mixture E_m:

$$E_m - h_v(p,\rho_v)(1-y_{hom}-y_{het}) - h_l(p)(y_{hom}+y_{het}) + \frac{p}{\rho_m} - \frac{1}{2}u_{mj}u_{mj} = 0 \quad (10)$$

The relation for pressure is of course non-linear due to the non-linear form of the applied equations of state for vapor and liquid (Eq. 3), and is solved by means of the Newton iteration method.

In this model, the volume of the condensate is neglected. Thus, the density of the vapor phase is calculated from the mixture density and the wetness fraction only. Next, knowing the pressure and the vapor density, the temperature of the vapor phase is calculated from the equation of state (Eq. 3).

The liquid temperature is calculated from the relation proposed by Gyarmathy [4]:

$$T_l = T_s(p) - (T_s(p) - T_v)\frac{r^*}{r} = T_s(p) - \Delta T\frac{r^*}{r} \quad (11)$$

The system of URANS equations coupled with the two equations turbulence model and equations (8) was differentiated in space using the finite volume method and integrated in time by means of the Runge-Kutta method [7, 10].

Numerical modeling was performed assuring the grid independent solution, with the dimensionless distance from the wall, $y+\approx 1...5$. The unsteady calculations were carried out with the constant time step $\triangle t = 10^{-8}$s.

4. Results

The boundary conditions for D1 nozzle at the inlet correspond to total pressure with the value of $96{,}000^{\pm 200}$ Pa(a) and temperature of $108^{\pm 0.25}$ °C. Back pressure at the nozzle outlet was about 40,000 Pa(a). Except for the total parameters the static pressure measurements along the nozzle straight wall together with Schlieren pictures were carried out during the experimental campaign.

Fig. 3 shows a comparison of the static pressure distribution obtained from numerical simulation with experimental data. The location of the condensation shock is well modeled, as can be seen, whereas its intensity is overpredicted in numerical calculations. The shock wave for this case is located at the nozzle outlet, behind the static pressure tubes. The location of the shock wave is also well modeled using the applied CFD code (Fig. 4). The strong separation in the place of shock wave interaction with the curve wall is depicted in Fig. 4. Due to this separation a lot of coarse water downstream of the shock wave is created. This might be a result of detachment of the water film on the nozzle wall, but also on the side wall made of polycarbonate. It affects the instability of the shock wave.

Since the applied numerical algorithm does not model water film formation or its behavior, the effects observed in experiment were not confirmed by numerical simulation. The calculated distribution of the wetness fraction (Fig. 5) shows partial evaporation of the liquid phase on the shock wave, and in the region where the coarse water was observed the modeled liquid phase has minimal values.

In the case of nozzle D1 the unsteadiness observed in the experiment does not affect the measured static pressure upstream of the shock wave.

For D2 nozzle at the inlet total pressure was $112{,}500^{\pm 250}$ Pa(a) and temperature $111^{\pm 0.25}$°C. Back pressure at 50,000Pa(a) was higher than for D1 nozzle. These boundary conditions determine the loca-

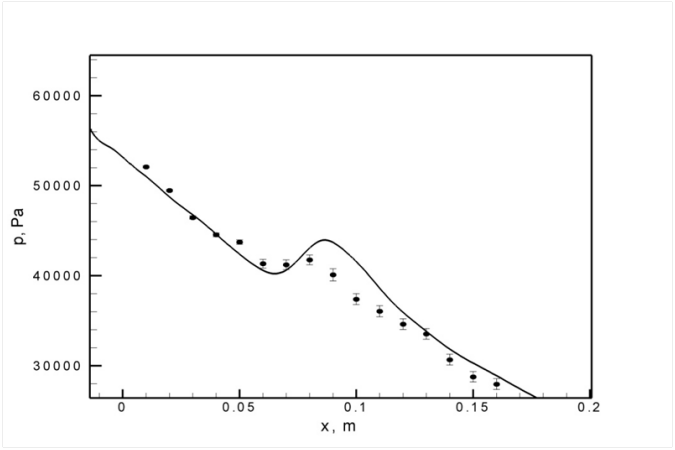

Figure 3: The static pressure distribution along straight wall of the D1 nozzle, comparison of the numerical results (solid line) with experiment (black dots)

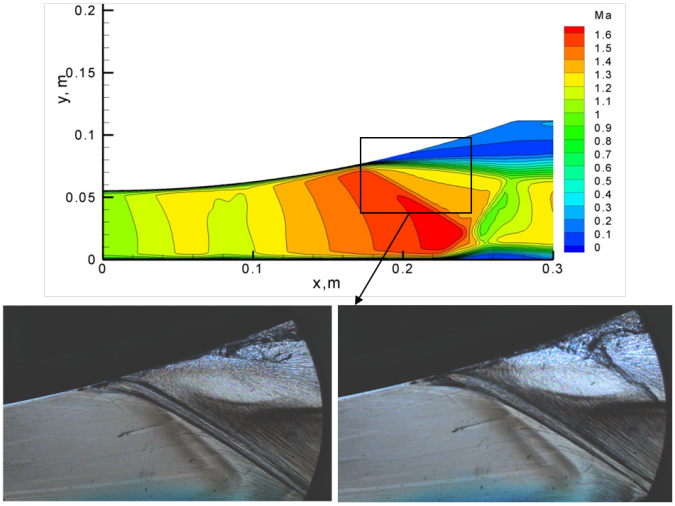

Figure 4: Calculated Mach number distribution (top) and Schlieren pictures from experiment for D1 nozzle

tion of the shock wave further upstream than in the previous case, which confirms the static pressure distribution depicted in Fig. 6.

The measured values of static pressure in the shock wave vicinity have much higher error, calculated as the sum of sensor accuracy and the difference between maximum and minimum values measured within 30 s with a frequency of 400 Hz. Condensation onset is well predicted in the numerical model, compared with experimental data.

In the shock wave region there are big discrepancies between the experimental results and calculations. This is due to the applied numerical model, which is not able to model the coarse water and water films

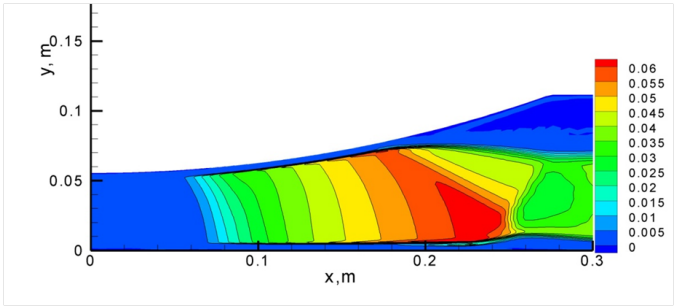

Figure 5: Calculated wetness fraction for D1 nozzle

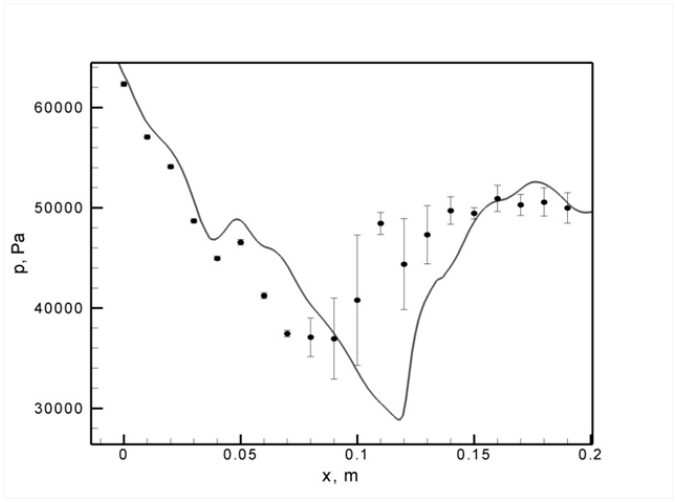

Figure 6: The static pressure distribution along straight wall of the D1 nozzle, comparison of the numerical results (solid line) with experiment (black dots)

on the solid walls. The position of the shock wave in numerical modeling is very stable (Fig. 7).

The calculated wetness fraction for the D2 nozzle (Fig. 8) confirms partial evaporation of the water on the shock wave and the absence of the liquid phase (in the form of coarse water observed in experiments) in the strong detachment region behind the shock wave in the area adjacent to the top wall.

5. Summary and conclusion

The paper comprises both experimental and numerical results of a steam condensing flow in the Laval nozzles. The effect of homogeneous condensation and shock wave behavior in the wet steam region was investigated.

The obtained experimental and numerical results led to the following conclusions:

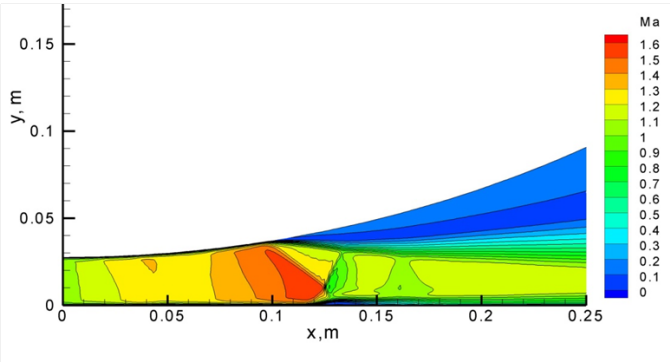

Figure 7: Calculated Mach number distribution for D2 nozzle

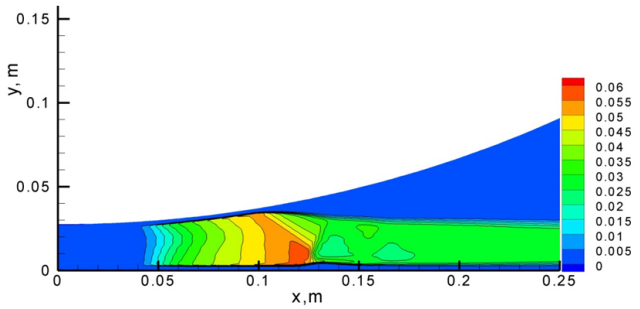

Figure 8: Calculated wetness fraction for D2 nozzle

1. The experiments investigating shock wave behavior in the wet steam region showed coarse water formation in the detachment zone
2. The presence of coarse water behind the shock wave is probably caused by water film separation on the nozzle walls and side walls
3. The effect of the corner between the nozzle wall and side wall in the process of strong coarse water formation has to be taken into account and analyzed more deeply
4. The modeling of the steam condensing flows with shock waves needs a much more sophisticated numerical model including water film formation and behavior
5. The applied numerical single-fluid model is able to predict condensation onset properly, but this model cannot properly model shock waves in the wet steam region
6. The small discrepancy between the calculated and measured static pressure distribution in the vicinity of the condensation shock may be a result of steam impurities that contribute to the mixed homo/heterogeneous condensation process

Future experimental work will concentrate on a detailed explanation of the phenomenon of coarse water formation in the separation region caused by the shock wave. This phenomenon could be crucial for further research concerning the nozzle and in particular linear cascades.

The work on numerical modeling will focus on the development of a two-fluid model that takes into account the velocity slip between liquid and gaseous phases.

Acknowledgements

The presented work was supported by National Science Center funds under PBU-7/RIE5/2012.

References

[1] J. Kotowicz, M. Job, Optimization of the steam part parameters in the GTCC unit with oxy-combustion and the carbon capture installation, Rynek Energii 107 (4) (2013) 48–55.

[2] M. Deich, Tsiklauri, G.V., V. Shanin, Danilin, V.S., Investigation of flows of wet steam in nozzles, Teplofizika Vysokikh Temperatur 1 (1972) 120–129.

[3] T. Krol, Results of optical measurement of diameters of drops formed due to condensation of steam in a laval nozzle., Trans. Inst. Fluid Flow Machinery (Poland) 57 (1971) 19–30.

[4] G. Gyarmathy, Grundlagen einer theorie der nassdampfturbine, Dissertation, Zurich, juris Verlag (1960).

[5] S. Dykas, Numerical calculation of the steam condensing flow. task quarterly, Scientific Bulletin of Academic Computer Centre, Gdańsk 5 (4).

[6] M. Heiler, Instationare phanomene in homogen/heterogen kondensierenden dusen- und turbinenstromungen, Dissertation, Universitat Karlsruhe (1999).

[7] W. Wróblewski, S. Dykas, A. Gepert, Modelling water vapour flow with heterogeneous condensation (in Polish), no. 95, Wydawnictwo Politechniki Śląskiej, Gliwice, 2006.

[8] K. Smołka, M. Strozik, M. Majkut, S. Dykas, Możliwości badań eksperymentalnych przepływu pary mokrej w układzie mini-siłowni kondensacyjnej, Vol. 27, Oficyna Wydawnicza Politechniki Warszawskiej, 2011, pp. 233–240.

[9] S. Dykas, W. Wróblewski, H. Łukowicz, Prediction of losses in the flow through the last stage of low pressure steam turbine, International Journal for Numerical Methods in Fluids 53 (2007) 933–945.

[10] W. Wróblewski, S. Dykas, A. Gardzilewicz, M. Kolovratnik, Numerical and experimental investigations of steam condensation in lp part of a large power turbine, ASME J. of Fluids Eng. 131.

[11] J. Frenkel, Kinetic theory of liquids, Oxford University Press, New Jork.
[12] A. Kantrowitz, Nucleation in very rapid vapour expansions, The Journal of Chemical Physics 19 (1951) 1097–1100.